Hexafluoroarsenates of Graphite from its Interaction with AsF_5, $AsF_5 + F_2$, and O_2AsF_6, and the Structure of $C_{14}AsF_6$

Fujio Okino *,† **and Neil Bartlett**

The Department of Chemistry and The Materials and Chemical Sciences Division of The Lawrence Berkeley Laboratory, The University of California, Berkeley, CA 94720, USA

The F:As molar ratio for the vacuum-stable products obtained following treatment of graphite, at room temperature, with (1) AsF_5, (2) $AsF_5 + F_2$, and (3) O_2AsF_6, has been established to be 6. X-Ray absorption spectra, in the arsenic-K pre-absorption edge region, indicate that the guest species in the vacuum-stable products *via* route (1) is AsF_6^-. Route (1) gives mixtures of stage-one and -two salts whereas (2) and (3) readily yield stage-one materials. This is attributed to the greater oxidizing potential of the reagents in (2) and (3). The volatiles from route (1) are AsF_5 and AsF_3, and from (2) AsF_5. The *c*-axis repeat distance (I_c) of the vacuum-stable hexafluoroarsenates of formula $C_{14n}AsF_6$ (where *n* is the stage) is *ca.* 7.6 + 3.35(n − 1) Å. X-Ray powder diffraction data for $C_{14}AsF_6$ ($I_c \approx 7.6$ Å) indicate that the fluoride ligands of AsF_6^- are nestled in contiguous three-fold sets of carbon atom hexagons of the graphite. This requires a staggering of the enclosing carbon layers. Adjacent pairs of carbon atom sheets contain assemblies of AsF_6^- of short range order. The ordered anion arrangement is that of closest packing for nestled AsF_6^-. Aside from the restriction imposed by AsF_6^- nestling, the carbon layers are randomly stacked. In cases where the graphite galleries are richer in arsenic fluoride guests (C_xAsF_y; $8 \leqslant x < 14$, $5 \leqslant y \leqslant 6$), the I_c distances are larger (*ca.* 8.0 Å) and the enclosing carbon layers are eclipsed.

Graphite–AsF_5 intercalation compounds[1] have aroused much interest particularly because of their high electrical conductivities.[2,3] A central issue, on which there has been much controversy, and which is crucial to any accounting of conductivity and other physical properties, has concerned the nature of the guest species in the graphite. Although there has been much effort to elucidate the nature of the guest species based on physical measurements,[4–8] precise compositional aspects of the preparations have been widely neglected. X-Ray arsenic pre-absorption edge studies by Bartlett *et al.*[9,10] had previously established that the intercalation of graphite by AsF_5 was accompanied by electron oxidation of the graphite according to equation (1). The implications of this for the preparation of

$$\tfrac{3}{2}AsF_5 + e^- \longrightarrow AsF_6^- + \tfrac{1}{2}AsF_3 \qquad (1)$$

graphite–AsF_5 intercalation compounds, and thus for their physical properties, have not been fully comprehended.

Falardeau *et al.*,[11] using X-ray diffraction, gravimetry and *c*-axis thickness measurements on highly oriented pyrolytic graphite (HOPG) intercalated samples, characterized graphite–AsF_5 intercalation compounds by the formula $C_{8n}AsF_5$ with $I_c = 4.75 + 3.35n$ Å, which transforms to $8.10 + 3.35(n - 1)$ Å. In such studies weight changes have usually been attributed to the uptake or loss of AsF_5. Loss of AsF_3 has usually not been taken into consideration. Consequently the products of the interaction of graphite with AsF_5 are almost invariably described as C_xAsF_5. Although allowance has generally been made for conversion of AsF_5 into AsF_6^- and AsF_3, the overall formulation of the product has generally been C_xAsF_5, *i.e.*, it has been assumed that AsF_3 remained in the product. Moran *et al.*[7] had observed previously that the I_c of freshly made stage-one C_xAsF_5 samples decreased as much as 0.5 Å (*e.g.*, from *ca.* 8.2 to 7.77 Å) when samples were evacuated. Based on weight loss measurements and the F:As ratio determined by X-ray photoelectron spectroscopy (XPS) for the residual compounds, they have claimed that the composition went from C_8AsF_5 to $C_{20}AsF_5$ losing only unreacted AsF_5, but no explanation was provided for the small I_c distance.

The first tasks of the work described in this paper were to define the chemical compositions of the vacuum-stable products derived from the interaction of graphite with AsF_5, AsF_5 mixed with F_2, and O_2AsF_6. The second tasks were to explain the peculiar features of the X-ray powder diffraction (XRPD) pattern for the stage-one $C_{14}AsF_6$ ($I_c \approx 7.6$ Å). A novel structure involving fluoride ligand nestling of the AsF_6^- in the hexagonal depressions of the carbon atom sheets is proposed.

Results and Discussion

Chemical Composition.—Since much of the controversy arising from work on graphite–AsF_5 materials derives from the scant attention paid to the chemical composition of the solid products and to the identity and the amount of the volatiles removed following intercalation, the discussion which follows includes an extended examination of these crucial concerns.

The IR spectra of the volatiles, from the product, *ca.* C_8AsF_5, made by the interaction of graphite with a single treatment of AsF_5, are compared with the spectra of gaseous AsF_5 and AsF_3 in Fig. 1.‡ Fig. 2 illustrates a typical weight loss curve for a C_8AsF_5 sample giving up volatiles in a dynamic vacuum. The IR spectra seldom revealed the presence of carbon fluorides in the volatiles from C_xAsF_5 samples. The assumption was therefore made that, during evacuation, no carbon containing

† *Present address:* Department of Chemistry, Faculty of Textile Science and Technology, Shinshu University, Ueda 386, Japan.

‡ The possibility that AsF_3 was observed as a product of reduction of AsF_5 by the materials of the vacuum line or the IR cell after the AsF_5 had left the product was ruled out by blank experiments. Gaseous AsF_5 (AsF_3-free by IR spectroscopy) was transferred from an empty reaction vessel to the IR cell. Arsenic trifluoride was not detected in the AsF_5 thus transferred. The transfer of AsF_5 was, however, not quite quantitative. When the amount of AsF_5 was very small, no IR spectrum was observed after the supposed transfer. This small absorption of AsF_5 is presumed to result from interaction of that acid fluoride with the metal fluorides covering the inner wall of the vacuum line: *e.g.* $NiF_2 + AsF_5 \longrightarrow NiF^+AsF_6^-$ or $NiF_2 + 2AsF_5 \longrightarrow Ni[AsF_6]_2$.

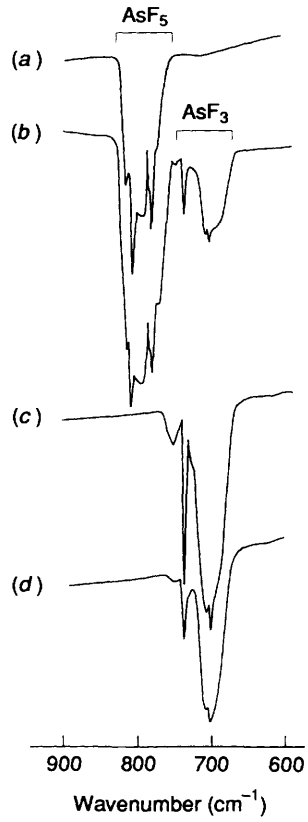

Fig. 1 Infrared spectra of AsF_5(g), AsF_3(g) and volatiles from *ca.* C_8AsF_5: (*a*) pure AsF_5(g) used for reaction; (*b*) first volatiles from solid *ca.* C_8AsF_5; (*c*) volatiles after several minutes of evacuation; and (*d*) pure AsF_3(g)

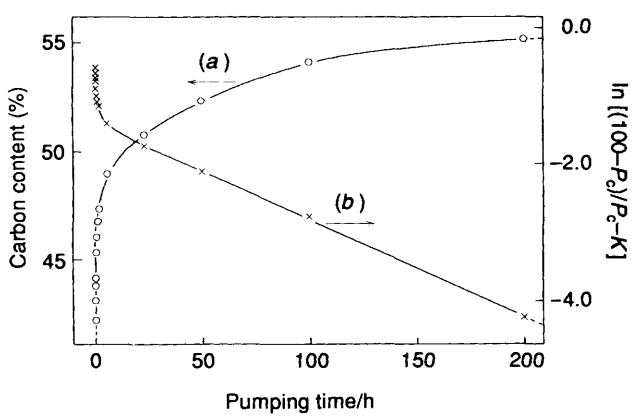

Fig. 2 (*a*) Loss of AsF_5 and AsF_3 represented by carbon content, P_C, increase as a function of pumping time, *t*, from the stage-one material of initial composition *ca.* C_8AsF_5. (*b*) Plot of $\ln[(100 - P_C)/P_C - K]$ *vs.* *t*; *K* (see text) was adjusted to yield a linear relationship for $t > 24$ h

gaseous species were lost. This was generally supported by the close agreement between the carbon content based on gravimetry and that from chemical analysis.

The composition of the solid product, after the initial removal of the gases, was usually close to $C_{10}AsF_{5+\delta}$ ($0 < \delta \ll 1$), corresponding to a carbon content of *ca.* 40%. Materials made in this way have been usually reported as $C_{10}AsF_5$.[1,4,5,12,13] However, the F:As ratio must be larger than 5:1, since evolution of AsF_3 has occurred. Even if a sample has never left an AsF_5 atmosphere, its composition must be expressed by $C_xAsF_{5+\delta}$ since some AsF_3, produced according to equation (1), enters the gaseous AsF_5 phase. The loss of AsF_3 from the graphite depends upon the relative quantities of the reactants and upon the reaction time. Such loss, however, can be small, as the analytical data of Pentenrieder and Boehm indicate.[14]

After several minutes of evacuation, AsF_5 was usually not observed in the IR spectrum. After 200 h of evacuation the carbon content of the sample, as illustrated in Fig. 2, became 55.2%, which, assuming the remaining guest species is AsF_6^-, corresponds to $C_{19.4}AsF_6$. The dominant volatile in the earlier stages of evacuation was AsF_5, with AsF_3 eventually becoming the only detectable volatile (after 4 h). It is probable that small quantities of AsF_5 continued to be evolved far into the evacuation (the gravimetric data indicate this), but, because of the absorption by the metal vacuum line and cell, these small quantities of AsF_5 were not detected by IR spectroscopy.

Also shown in Fig. 2 is a plot derived based on the assumption that the loss of volatiles follows first-order kinetics except for the initial period. Using P_C (carbon content in weight percent) and *t* (time in h), we obtain expression (2) where λ is the

$$\ln\left(\frac{100 - P_C}{P_C} - K\right) = -\lambda t + b \qquad (2)$$

rate (decay) constant, *K* [equation (3)] is the weight ratio of

$$K = \ln\frac{\text{formula weight of } AsF_6^-}{x(\text{atomic weight of carbon})} \qquad (3)$$

AsF_6^- to carbon in the final ($t = \infty$) product, C_xAsF_6 and *b* is the logarithm of the weight ratio of volatiles to carbon in the initial sample, $C_xAsF_6{\cdot}\delta(AsF_5, AsF_3)$ given by expression (4).

$$b = \ln\frac{\text{weight of } \delta(AsF_5, AsF_3)}{x(\text{atomic weight of carbon})} \qquad (4)$$

The value of *K*, consequently, *x* in C_xAsF_6 (at $t = \infty$) was adjusted to make the data follow first-order kinetics, and the best fit was obtained for $x \approx 20$ ($C_{20}AsF_6$, 56% carbon by weight); λ is calculated to be 1.4×10^{-2} h^{-1} (half-life: 49 h). This implies that the ionization extent[6,7] *of a single treatment* of graphite with AsF_5 is *ca.* C_{20}^+.

Since compositions cannot be determined accurately by gravimetry alone, chemical analyses (C, H, N, As, F and O) were carried out on the vacuum-stable products. The results are shown in Table 1. It shows that interaction of graphite with AsF_5 alone is an effective route to the production of C_xAsF_6 salts, so long as care is taken to remove the volatiles completely. After several cycles the stage-one phase was in much greater concentration than the stage-two phase, whereas the reverse was true for one cycle. However, the repeated treatment of graphite with AsF_5 alone, followed by evacuation, never leads to pure stage-one products.

The X-ray arsenic K-shell pre-absorption edge feature [As(1s → 4p) transition] for the vacuum-stable product, *ca.* $C_{19}AsF_6$, prepared from graphite and AsF_5 followed by evacuation, gave the single peak feature shown in Fig. 3, and indicates that AsF_6^- is the sole guest species in a vacuum-stable sample. This contrasts with the double peak feature reported by Bartlett *et al.*[9,10] for the material from which volatiles had not been removed, and which was characteristic of a mixture of AsF_3 and AsF_6^- species.

It had been reported[7,8] that, when C_xAsF_5 was evacuated, the I_c decreased markedly (*ca.* 0.5 Å), but only over a long period of evacuation. The nature of this decrease in I_c distance was not adequately accounted for nor fully investigated. As is shown in Fig. 4, the present study reveals that the I_c of stage-two phases decreased more readily than those of stage-one phases upon evacuation. This is probably a consequence of there being many more voids and interconnected open channels in the stage-two materials. It is also noted that the decrease in I_c distance of samples treated by AsF_5 repeatedly was more rapid than for

Table 1 Analytical data and I_c distances for the vacuum-stable solid products obtained from (1) graphite + AsF_5, (2) graphite + AsF_5 + F_2, and (3) graphite + O_2AsF_6

		Analysis[a] (%)								
Reactants	Method	C	H	As	F	N	O	C + As + F	Composition	I_c/Å
(1) C + AsF_5	One cycle	56.12	0.70	17.26	26.30	<0.001	<0.5	99.68	$C_{20.28}AsF_{6.01}$	7.64
	Six cycles	50.15	0.05	19.63	29.79	0.003	—	99.57	$C_{15.94}AsF_{5.98}$	7.84
(2) C + AsF_5 + F_2	—	45.09	0.09	21.56	32.85	0.010	<0.5	99.50	$C_{13.05}AsF_{6.01}$	7.71
(3) C + O_2AsF_6	(*a*)[b]	46.96	0.21	20.91	31.85	0.023	<0.3	99.72	$C_{14.01}AsF_{6.01}$	7.57
	(*a*)[b]	51.79	<0.01	19.05	28.98	0.001	<0.3	99.82	$C_{16.96}AsF_{6.00}$	7.56
	(*c*)[b]	43.42	0.11	22.23	33.78	0.001	<0.5	99.43	$C_{12.81}AsF_{5.99}$	7.75

[a] Experimental values determined by Galbraith Laboratories, Inc. [b] See text for methods (*a*) and (*c*).

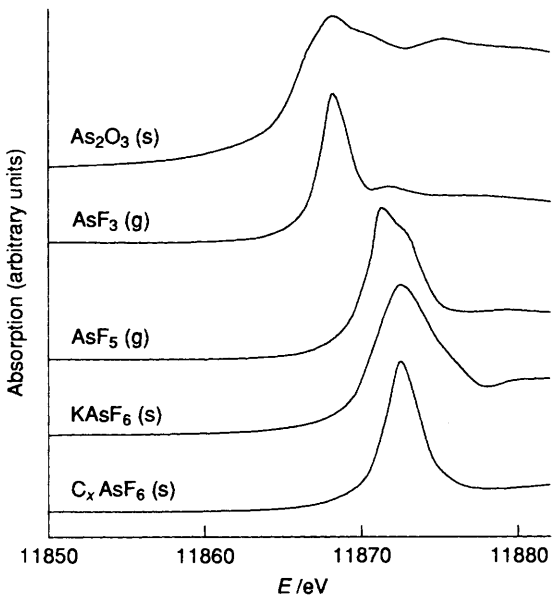

Fig. 3 Chemical shifts in the arsenic K-shell pre-absorption edge feature (1s → 4p transition) for C_xAsF_6 and the relevant materials (eV ≈ 1.6 × 10^{-19} J)

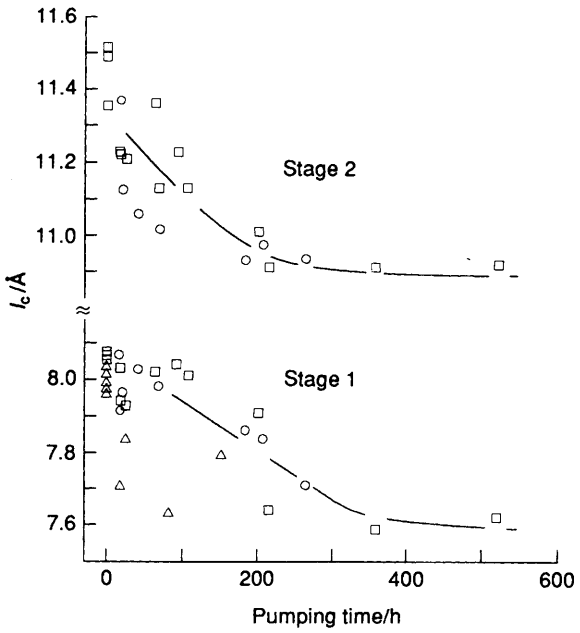

Fig. 4 The relationship between the I_c distance and the pumping time, *t*, for graphite intercalated by AsF_5 (and F_2); C + AsF_5 (□), C + AsF_5 repeated treatments (○), C + AsF_5 + F_2 (△). For those samples repeatedly treated with AsF_5, the pumping time is measured from the last cycle

those treated once. This is probably a consequence of most of the slow-moving AsF_3 having been removed in the first evacuation.

The ready loss of AsF_5 stands in marked contrast to the very slow removal of AsF_3, and calls for comment. The AsF_5 can form $As_2F_{11}^-$ with AsF_6^-,[15] and an AsF_5 molecule can thereby be generated in a new location without actual translational movement of the molecule [equation (5)].

$$*AsF_5 + AsF_6^- \longrightarrow [*AsF_5\text{–}F\text{–}AsF_5]^- \longrightarrow *AsF_6^- + AsF_5 \quad (5)$$

On the other hand, AsF_3, being a much inferior fluoride ion acceptor than AsF_5, does not have such a mechanism for effective transfer available to it. Jostling of the AsF_3 molecules through a relatively close-packed environment is evidently slow. Some AsF_3 interacts slowly with AsF_6^- to generate AsF_5 [reverse of equation (1)], which can then be rapidly transported.

In order to find an effective route to pure stage-one salts, the interaction of graphite with AsF_5 + F_2 was studied. The results in Table 1 show that a pure stage-one C_xAsF_6 salt was produced by this route. Fig. 4 clearly indicates that the I_c distance decrease upon evacuation in these samples is very rapid compared with that of those made from graphite and AsF_5 alone. No AsF_3 was observed in the volatiles during the evacuation process, and this absence of AsF_3 in the galleries is probably the reason for the rapid decrease in I_c distance. This is because the formation of the C_xAsF_6 salt has occurred by the oxidation represented by equation (6). Loss of AsF_5, CF_4 and SiF_4 (the last two seldom seen in the intercalation by AsF_5 alone) must be the cause of the decreases in both I_c distance and weight.

$$AsF_5 + \tfrac{1}{2}F_2 + e^- \longrightarrow AsF_6^- \quad (6)$$

When graphite is treated with O_2AsF_6 in SO_2ClF as a solvent, a stage-one salt with the composition *ca.* $C_{14}AsF_6$-$(SO_2ClF)_{0.5}$ is formed contrary to the previous reports.[9,10] This loses SO_2ClF slowly in a dynamic vacuum but the process appears to be reversible. To circumvent the added complexity caused by SO_2ClF incorporation, the C_xAsF_6 salts were prepared by the direct interaction of graphite with solid O_2AsF_6. Although slow, the reactions proceeded to completion when the two solids were mixed well by mechanical agitation. The results of chemical analyses on these compounds are summarized in Table 1. They show that C_xAsF_6 salts were formed. This is in accordance with the oxidative reaction (7).

$$O_2AsF_6 + e^- \longrightarrow AsF_6^- + O_2 \quad (7)$$

A plot of I_c distance against the composition, *i.e.* against *x* in

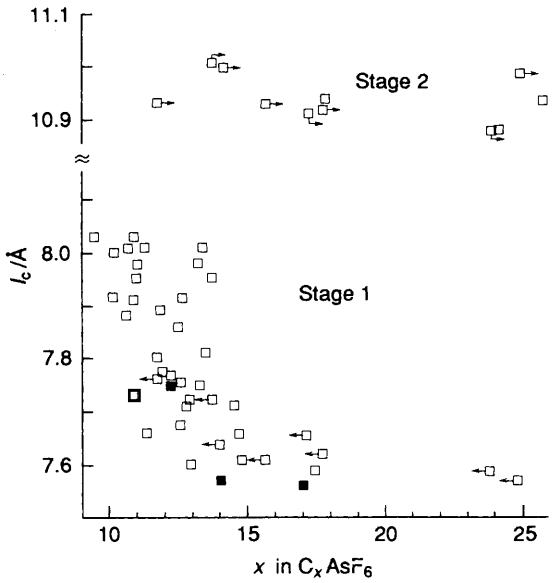

Fig. 5 The relationship between the I_c distance and the carbon content of the samples made by the reaction of graphite and O_2AsF_6(c) (The values of x were calculated based on carbon analyses assuming the formula C_xAsF_6. The samples with filled squares were confirmed to be $C_xAsF_{5.99-6.01}$ by C, H, N, As, F and O analyses. Arrows in the figure indicate materials which were mixtures of stage-one and -two phases. For such materials the pure stage-one and -two phases in each sample must have smaller and larger values of x, respectively)

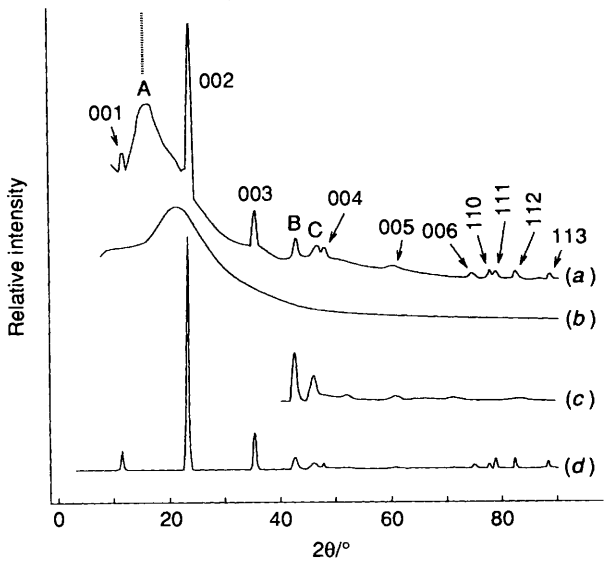

Fig. 6 (*a*) Observed Debye–Scherrer X-ray powder diffraction patterns (Cu-Kα) of the nestled $C_{14}AsF_6$, (*b*) quartz capillary background, (*c*) calculated (10*l*) diffuse scattering, (*d*) simulated pattern with (00*l*) and (11*l*) crystal reflections, and (10*l*) diffuse scattering

C_xAsF_6 is shown in Fig. 5.* The figure indicates very clear trends: (*i*) stage-two phases always have a small I_c distance of 10.9 Å (which corresponds to 7.55 Å for stage-one); (*ii*) stage-one phases also have a small I_c distance (7.6 Å), when $x \geqslant 14$, (*iii*) stage-one phases with $x < 14$ have a larger I_c distance (7.6–8.0 Å); (*iv*) the limit of x in C_xAsF_6 appears to be *ca.* 10. Although Fig. 5 does not show it, the composition of the pure stage-two material, in which the other stage phases were not detectable by XRPD, was *ca.* $C_{28}AsF_6$. These observations indicate that the vacuum stable C_xAsF_6 salts with the I_c distance of *ca.* 7.6 + 3.35*n* Å have the staging formula $C_{14+x}AsF_6$.

Milliken and Fischer[8] have argued that the ionization limit of a graphite host layer is *ca.* C_{20}^+, and that further oxidation in the graphite–AsF_5 system by the fluoride results in the formation of covalently bonded fluorine. As the analytical data in Table 1 show, however, the F : As atomic ratio in all of the vacuum-stable graphite salts is 6 : 1, for compositions ranging from C_{13}- to C_{20}-AsF_6. Therefore, even though the physical or electronic ionic salt limit in graphite–fluoroarsenate may be C_{20}^+, for the salts made by repetitive treatment with AsF_5, or for those made using stronger oxidizers, the chemical formulation, $C_x^+AsF_6^-$ ($x \leqslant 20$), should be valid.[16] This formulation is further supported by the low-temperature structure of $C_{16}^+AsF_6$.[17] It is also noted that the limiting (vacuum-stable) composition for the product *of single treatment* of graphite with AsF_5 is *ca.* $C_{20}AsF_6$. Formulating this as $C_{20}^+AsF_6^-$ gives a result in good agreement with the conclusions of Milliken and Fischer.[8]

Incorporation of AsF_5 *and* AsF_3 *in* C_xAsF_6 *Salts.*—For the materials prepared from graphite and AsF_5 for which $I_c \approx 8.0$ Å, the removal of volatiles leads to a vacuum-stable material with $I_c \approx 7.6$ Å. The latter represents a relatively ordered arrangement of the AsF_6^- species, they being nestled in the enclosing graphite honeycomb arrays. Addition of either AsF_3 or AsF_5 to the $C_{14}AsF_6$ markedly increases the I_c distance. Neither the AsF_6^- nor the neutral species is now nestled. The findings in Table 2 show that the limit of AsF_5 or AsF_3 incorporation agrees roughly with the formula $C_{14}AsF_6 \cdot \frac{1}{2}(AsF_5$ or $AsF_3)$.

The incorporation of gaseous species into graphite intercalation compounds signifies loss of entropy. The increase in lattice energy, which accompanies this incorporation of gaseous species, must provide for the spontaneity of the process, *i.e.*, $|\Delta H(\text{lattice energy})| \geqslant |T\Delta S|$. Evidently neutral species such as AsF_5, AsF_3 or SO_2ClF are acting as dielectric spacers. These spacers must reduce the anion–anion repulsion and in so doing more than compensate for the loss in Coulomb attraction energy associated with the *c*-axis expansion which, in these cases, is generally from 7.6 to 8.0 Å. Furthermore the ion–dipole or ion–induced dipole interaction ('solvation'[18] of the guest species) will favour the incorporation of gaseous species.

The Extent of Intercalation and the Oxidizing Power of the Guest Precursors.—The inability of AsF_5 alone with graphite to generate pure stage-one salts stands in marked contrast with the ready formation of such salts by $AsF_5 + F_2$, and O_2AsF_6. The basis for these differences appears to be thermodynamic. Free energy changes for related oxidizing half reactions (8)–(10) have been previously evaluated and are as follows (cal = 4.184 J).[19–23]

	$-\Delta G°_{298}$/ kcal mol^{-1}	
$\frac{3}{2}AsF_5(g) + e^- \longrightarrow AsF_6^-(g) + \frac{1}{2}AsF_3(g)$	125	(8)
$AsF_5(g) + \frac{1}{2}F_2(g) + e^- \longrightarrow AsF_6^-(g)$	170	(9)
$O_2AsF_6(c) + e^- \longrightarrow AsF_6^-(g) + O_2(g)$	155	(10)

The ready formation of pure stage-one salt, $C_{14}AsF_6$, by the oxidizers O_2AsF_6 and AsF_5–F_2, but the failure of AsF_5 to do likewise, can therefore be attributed to the greater oxidizing power of O_2AsF_6 and AsF_5–F_2. That this inferiority in oxidizing capability of AsF_5 is indeed thermodynamically and not kinetically based[24] is indicated by the product of the interaction of AsF_3 with stage-one salts $C_{14}AsF_6$ which had been prepared using either AsF_5–F_2 or O_2AsF_6. When the

* Some discrepancies in Fig. 5 can be explained by inhomogeneity in the samples, *e.g.*, even though the composition of the stage-one phase is C_xAsF_6 ($x < 14$), there may be a small domain of stage-two, and the sample may be metastable with respect to the conversion toward a mixture of two phases with smaller I_c distances, when the overall composition of the sample allows it, *i.e.* C_xAsF_6 ($x > 14$).

Table 2 Data relating to interactions of $C_{14n}AsF_6$ with AsF_5 and AsF_3

Sample	Treatment	Duration	% C	Composition[a]	I_c/Å stage-one/-two
1[b]			48.92	$C_{15.1}AsF_6$	7.61/—
	$+AsF_5$	15 h	38.21	$C_{15.1}AsF_6 \cdot 0.6AsF_5$	7.97/—
	Pump	60 h	48.72	$C_{15.1}AsF_6 \cdot 0.01AsF_5$	7.65/—
2[b]			48.92	$C_{15.1}AsF_6$	7.61/—
	$+AsF_5$	14 h	38.43	$C_{15.1}AsF_6 \cdot 0.6AsF_5$	7.97/—
	Pump	60 h	48.72	$C_{15.1}AsF_6 \cdot 0.05AsF_5$	7.65/—
3[c]			45.55	$C_{13.2}AsF_6$	7.71/—
	$+AsF_3$	4 d	37.24	$C_{13.2}AsF_6 \cdot 0.6AsF_3$	8.15/11.68
	Pump[d]	8 d	53.05	$C_{17.8}AsF_{6-\delta}$	7.65/10.92
4[e]			47.53	$C_{14.3}AsF_6$	7.71/—
	$+AsF_3$	2 d	41.73	$C_{14.3}AsF_6 \cdot 0.4AsF_3$	8.15/11.68
	Pump[d]	2 d	49.74	$C_{15.6}AsF_{6-\delta}$	7.65/10.92

[a] Compositions were determined based on % C (C, H, N analyses). They were given by assuming that the amount of AsF_6^- in each sample remained unchanged during the reaction processes, except for samples 3 and 4 after the evacuation. These compositions were consistent with the gravimetry, but this was not as precise as % C in fixing the composition. [b] Samples 1 and 2 were obtained in the same preparation from C + AsF_5 + F_2 system. [c] Obtained by the reaction of C + AsF_5 + F_2. [d] The IR spectrum of the volatiles indicated the presence of some AsF_5 in the initial volatiles removed. [e] Obtained by the interaction of graphite and O_2AsF_6.

Table 3 Observed and calculated $1/d^2$ values and possible indexing for one of the representative samples with I_c distance of *ca.* 7.6 Å of composition *ca.* $C_{14}AsF_6$. Observed 2θ values and those obtained from the simulation by the model are included. a_0 = 2.454(2) Å, I_c = 7.626(3) Å; composition *ca.* $C_{14}AsF_6$

	$1/d^2$		2θ	
hkl	Obs.	Calc.	Obs.	Simulated
001	0.0169	0.0171	11.50	11.57
A[b]	*ca.* 0.031	—	*ca.* 15.7	—
002	0.0683	0.0687	23.25	23.32
003	0.1541	0.1547	35.23	35.30
B[b]	0.2233	—	42.73	42.8
C[b]	0.2597	—	46.26	46.3
004	0.2753	0.2750	47.72	47.69
005	0.4287	0.4297	60.63	60.71
006	0.6194	0.6188	74.70	74.66
110	0.6635	0.6642	77.80	77.85
111	0.6813	0.6814	79.03	79.04
112	0.7324	0.7330	82.56	82.60
113	0.8205	0.8189	88.50	88.47

[a] Least-squares fitted. [b] See Fig. 6 for the line designations (A, B and C).

Table 4 Observed and calculated $1/d^2$ values and possible indexing for one of the representative samples with I_c distance of *ca.* 8.0 Å of composition *ca.* $C_{10}AsF_6$. a_0 = 2.460(1) Å, I_c = 7.999(2) Å; composition *ca.* $C_{10}AsF_6$

	$1/d^2$	
hkl	Obs.	Calc.*
001	0.0154	0.0156
002	0.0624	0.0625
003	0.1404	0.1407
100	0.2206	0.2204
004	0.2498	0.2361
102	0.2832	0.2830
103	0.3606	0.3612
005	0.3911	0.3910
104	0.4712	0.4707
006	0.5635	0.5630
110	0.6618	0.6614
111	0.6782	0.6771
112	0.7235	0.7240
113	0.8012	0.8022

* Least-squares fitted.

volatiles are removed from $C_{14}AsF_6 \cdot \frac{1}{2}AsF_3$, they include AsF_5. The vacuum-stable residual solid is a mixture of stage-one ($C_{14}AsF_6$) and stage-two ($C_{28}AsF_6$) salts, comparable to the mixture derived from the interaction of graphite with AsF_5 after an extended removal of volatiles. Clearly, in forming the stage-two phase within the bulk, AsF_3 acts as a reducing agent towards $C_{14}^+AsF_6^-$ [equation (11)].

$$2C_{14}AsF_6 + \tfrac{1}{2}AsF_3 \longrightarrow C_{28}AsF_6 + \tfrac{3}{2}AsF_5 \quad (11)$$

Structural Models[25]

The Debye–Scherrer (DS) XRPD data for stage-one $C_{14}AsF_6$* ($I_c \approx 7.6$ Å) are presented in Table 3 and Fig. 6, and those for C_xAsF_y ($8 \leqslant x \leqslant 14$, $5 \leqslant y \leqslant 6$,† $I_c \approx 8.0$ Å) are given in Table 4 and Fig. 7. The temperature dependence (300–390 K) of

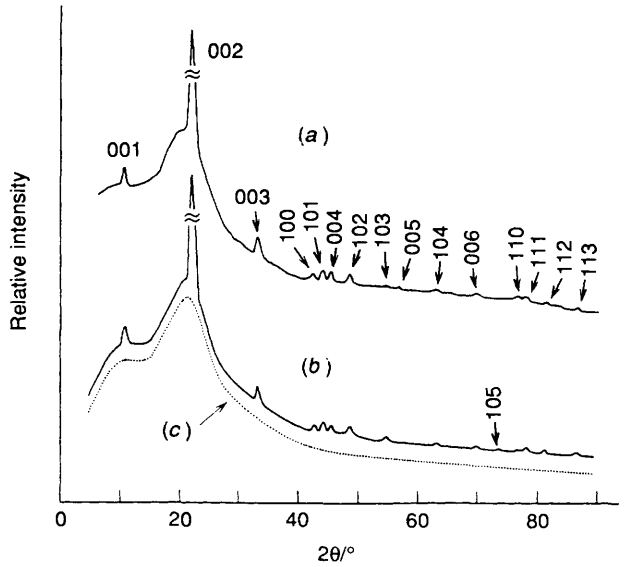

Fig. 7 (*a*) Observed Debye–Scherrer X-ray powder diffraction patterns (Cu-Kα) for the large I_c distance (*ca.* 8.0 Å) material of composition *ca.* $C_{10}AsF_6$, (*b*) calculated pattern, (*c*) quartz capillary background

* The composition of a sample need not be exactly $C_{14}AsF_6$ to produce the peculiar features discussed below in the text. The low-temperature Guinier–Simon data (ref. 17) suggest that the stage-one three-dimensionally ordered low-temperature phase has the composition $C_{16}AsF_6$.

† The conditions $8 \leqslant x < 14$ and $5 \leqslant y \leqslant 6$, for an unnestled stage-one sample should not be taken rigorously. For example, $C_{13}AsF_5$ will be a mixture of stages-one and -two, and C_8AsF_6 may not exist.

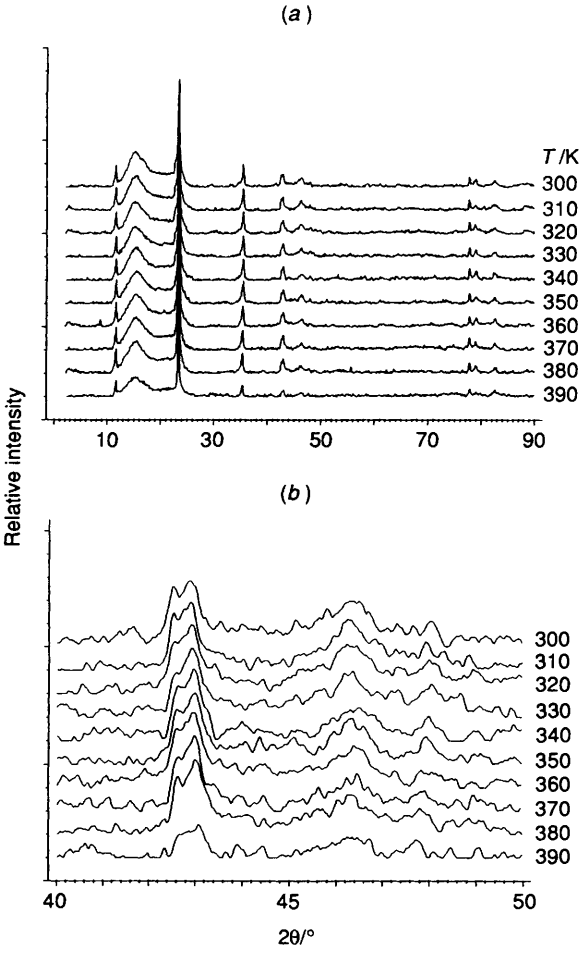

Fig. 8 Temperature dependence of the Guinier–Simon X-ray powder diffraction pattern (Cu-Kα_1) of *ca.* $C_{14}AsF_6$ between 300 and 390 K; (*a*) $0 < 2\theta < 90°$, (*b*) $40 < 2\theta < 50°$

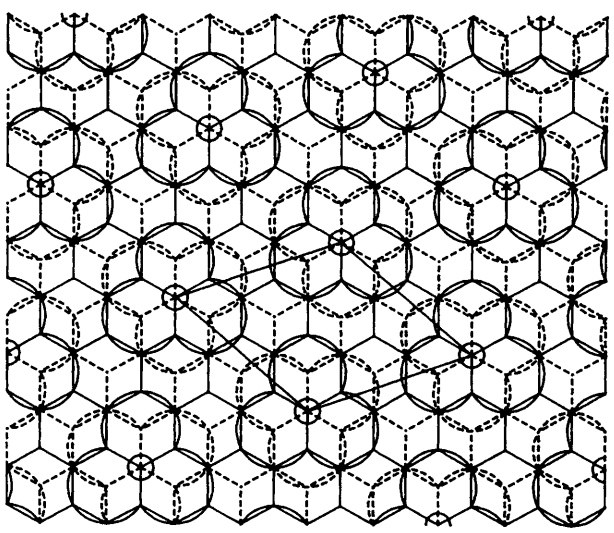

Fig. 9 Structure of $C_{14}AsF_6$. Requirement of staggering of carbon layers imposed by the nestling of AsF_6^- anions. Solid- and dashed-line fluorine atoms, respectively, are nestled in solid- and dashed-line carbon hexagonal nets

the XRPD pattern for $C_{14}AsF_6$ taken by the Guinier–Simon camera [26] is shown in Fig. 8.

Structural Model for $C_{14}AsF_6$.—When the two patterns of $C_{14}AsF_6$ and C_xAsF_y are compared, four features are notable for the former: (*i*) the I_c distance of 7.63 Å is appreciably smaller than that of C_xAsF_y ($I_c \approx 8.0$ Å); (*ii*) most of the lines are sharp and indexable as (00*l*), (110) or (11*l*) based on a graphite-like cell expanded along the *c* axis [$a_0 = a_0$(graphite), $c_0 = I_c = 7.63$ Å]; (*iii*) (100) and (10*l*) reflections are absent; and (*iv*) halo-like reflection, A, and somewhat broader reflections, B and C, are not indexable on the simple graphite-like cell. Line B is not (100); $1/d^2$ of line B is appreciably greater than one-third of that of (110). This relationship, $3/d^2_{100} = 1/d^2_{110}$, holds for C_xAsF_y.

Features (*i*) and (*iii*) gave the first pointers to the disposition of the AsF_6^- guests with respect to the carbon sheets. Since the effective thicknesses of the octahedral AsF_6^- ion along a three-fold axis [27–29] and a graphite carbon layer [30] are *ca.* 4.7 and 3.35 Å, respectively, the I_c distance of 7.6 Å between the carbon sheets requires that there be a 0.2 Å penetration of the anion into each enclosing graphite layer. This penetration can occur most effectively if a three-fold set of fluoride ligands of the anion nestle in a contiguous three-fold set of hexagons of the graphite, as illustrated in Fig. 9. As a consequence of the effective D_{3d} symmetry of the AsF_6^- in this environment the nestling requires the two enclosing graphite layers to be staggered with respect to one another (see Fig. 9).* The observed XRPD features, B and C, are simulated well by the model with randomly stacked carbon layers as shown in Fig. 6.

It, however, cannot account for the observed low-angle halo-like feature (A in Fig. 6), which suggests short-range ordering or domain structure [31] of the nestled AsF_6^- species in the graphite galleries. That the compositions of stage-one and -two graphite hexafluoroarsenates with small I_c values are $C_{14}AsF_6$ and $C_{28}AsF_6$, respectively, suggests that there is a particular in-plane arrangement of the nestled AsF_6^- species. Indeed, if AsF_6^- are nestled in a graphite sheet, fluoride ligands of two different AsF_6^- ions cannot be placed in adjacent hexagon sites because the sum of the van der Waals radii of the fluoride ligands greatly exceeds 2.46 Å. Therefore, for closest possible packing of such nestled species, carbon atom hexagons immediately adjacent to those containing nestled fluoride ligands must be vacant. The closest arrangement is that shown in Fig. 9. This accounts for the $C_{14}AsF_6$ stoichiometry. The (100) reflection of the unit cell [$a_0 = \sqrt{7}a_0$(graphite)] shown in Fig. 9 falls roughly at the centre of halo A as indicated by the dotted line above it in Fig. 6.

The simulation of the XRPD pattern for $C_{14}AsF_6$, however, was carried out without taking the in-plane arrangement of AsF_6^- into consideration, *i.e.*, in-plane statistical distribution of the nestled AsF_6^- was assumed. It was not incorporated because of the broadness of halo A and of the limited information obtainable from the XRPD data alone on the two-dimensional arrangement of the guest species. (Preparation of the nestled $C_{14}AsF_6$ using a single crystal of graphite has been unsuccessful so far.) Fig. 10 schematically represents the model for the random stacking of carbon layers with statistical distribution of nestled AsF_6^-.

In simulating the observed diffraction pattern, however, large values of anisotropic thermal parameters (U_{11}) were necessary for As and F atoms. The temperature dependence of the pattern obtained by the Guinier–Simon method (Fig. 8) indicates that the pattern essentially does not change up to 390 K. This hinted that there prevails considerable disorder already at room temperature. The fine structure at 300 K shown in Fig. 8(*b*)

* This raises the question of the carbon-layer stacking sequence. If the sequences were ordered, *i.e.*, if we had ABAB . . . or ABCABC . . ., the consequences of that ordering would be evident in the diffraction data. There is no evidence for such ordering. The ABAB sequence should produce easily detectable (10*l*) reflections based on a cell $a_0 = a_0$(graphite) and $c_0 = 2I_c$. No sharp reflection occurs but the required *d* spacing of (103) is close to that of line C. The ordered ABCABC sequence would explain the absence of (100), but neither of the sequences can account for line B nor the general absence of (10*l*) reflections.

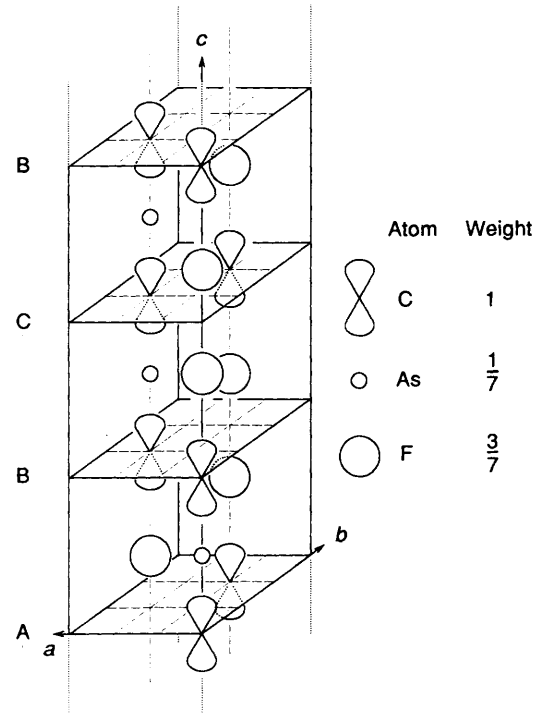

Fig. 10 Schematic representation of randomly stacked carbon layers with statistically distributed nestled AsF_6^- ions

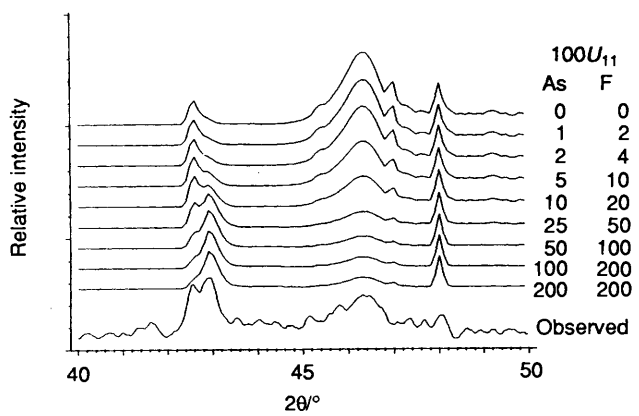

Fig. 11 Observed Guinier–Simon X-ray powder diffraction pattern (Cu-Kα_1) of the nestled $C_{14}AsF_6$ at 300 K and the dependence of simulated pattern on the anisotropic thermal parameters U_{11}(As) and U_{11}(F)

Table 5 Anisotropic thermal parameters* (× 100) used for the calculations

Model	Atom	U_{11}	U_{33}
Nestled $C_{14}AsF_6$	C	2	2
($I_c \approx 7.6$ Å)	As	25	5
	F	50	10
Unnestled $C_{10}AsF_6$	C	2	2
($I_c \approx 8.0$ Å)	As	—	6
	F	—	16

* The anisotropic thermal parameter expression used is $\exp[-2\pi^2(U_{11}h^2a^{*2} + U_{22}k^2b^{*2} + U_{33}l^2c^{*2} + 2U_{12}hka^*b^* + 2U_{13}hla^*c^* + 2U_{23}klb^*c^*)]$. U_{ij} thermal parameters expressed in terms of mean-square amplitude of vibration in angstroms (Å^2).

aided the adjustment of the values. The dependence of the simulated fine structure on the values of the anisotropic

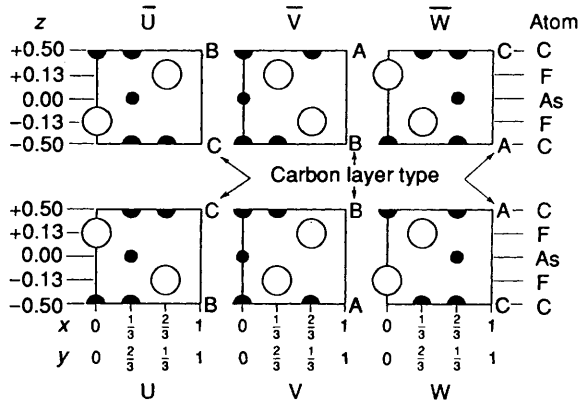

Fig. 12 Schematic representation of the six cells ±U, ±V and ±W used in the $C_{14}AsF_6$ model

parameters U_{11} is shown in Fig. 11. A satisfactory fit was obtained when U_{11}(As) = 0.25 and U_{11}(F) = 0.50 Å^2. The anisotropic thermal parameters used for the calculation are summarized in Table 5. Although the values necessary for the simulation are relatively large for U_{11}(As) and U_{11}(F), the fact that the larger values do not simulate the fine structure supported the AsF_6^- nestling.

The model shown in Fig. 10 together with the anisotropic thermal parameters given in Table 5 produces pattern (*d*) in Fig. 6 which is the combination of the crystal reflections, (00*l*) and (11*l*), where *l* takes integral values, and the diffuse scattering (10*l*), where *l* is a continuous variable, depicted by pattern (*c*). The excellent agreement gives strong support for the model of nestled AsF_6^-. Further support for the AsF_6^- nestling comes from the low-temperature (80–290 K) Guinier–Simon data, which indicate a three-dimensionally ordered nestled phase, $C_{16}AsF_6$, below 170 K.[17]

Mathematical Treatment of the Model for $C_{14}AsF_6$.—In this section the outline of the mathematical derivations for the model is given.[25,32,33] In order to treat the model mathematically, the model was conceived of as random stacking of the six cells (±U, ±V and ±W, where ±X = [X and $\bar{X}$]) shown in Fig. 12. The structure factors for cells ±V are expressed by equation (12), where $\alpha = 2\pi(h - k)/3$. $F_{\pm U}$ and $F_{\pm W}$ are given

$$F_{\pm V} = \tfrac{1}{7}\{f_{As} + 6f_F\cos(\alpha \pm 2\pi/z_F) + 7[f_C\cos \pi l + \cos(\alpha \pm \pi l)]\} \quad (12)$$

by $F_{\pm U} = F_{\pm V}\exp 2\pi i\alpha$ and $F_{\pm W} = F_{\pm V}\exp(-2\pi i\alpha)$. The stacking scheme starting with cell V is shown in Fig. 13. This kind of treatment, somewhat different from the usual treatment of planar disorders, was necessary, since two sets of AsF_6^- between, for example, AB- and BA-stacked graphite layers are not related by translation alone.

Letting $\bar{F}$ be the average value of the structure factors of the unit cells, and setting $F_n = \bar{F} + \varphi_n$ leads to equation (13)

$$F_nF^*_{n+m} = \bar{F}^2 + \overline{\varphi_n\varphi^*_{n+m}} = \bar{F}^2 + \Phi_m \quad (13)$$

where $\overline{\varphi_n} = \overline{\varphi_{n+m}} = 0$ was used, and $\overline{FF^*}$ was abbreviated by $\bar{F}^2$. Then the intensity I for the model, expressed in electron units, can be divided into two terms; the usual Laue–Bragg (crystal) reflections, I_{CR}, arising from $\bar{F}^2$, and the diffuse scattering, I_{RS}, from the random stacking [equations (14) and (15)] where N_1, N_2 and N_3 are the numbers of cells along

$$I_{CR} = \frac{\sin^2\pi N_1h}{\sin^2\pi k}\cdot\frac{\sin^2\pi N_2k}{\sin^2\pi k}\cdot\frac{\sin^2\pi N_3l}{\sin^2\pi l}\bar{F}^2 \quad (14)$$

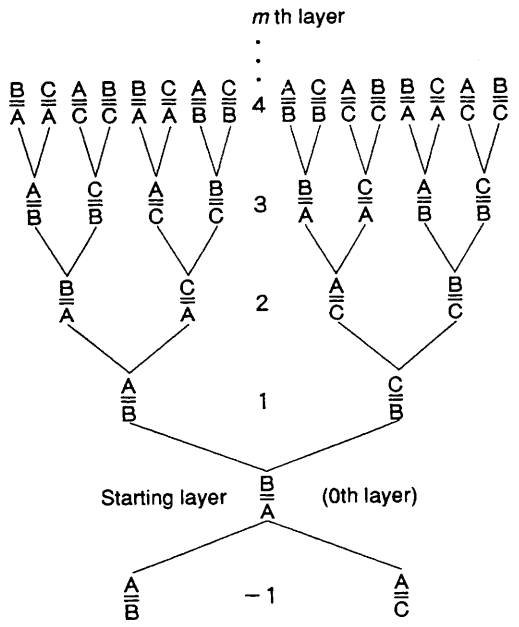

Fig. 13 Random stacking sequences of the cells starting with cell V

$$I_{RS} = \frac{\sin^2\pi N_1 h}{\sin^2\pi h} \cdot \frac{\sin^2\pi N_2 k}{\sin^2\pi k} N_3 \sum_m \Phi_m \exp(2\pi i l m) \quad (15)$$

the a, b and c axes, respectively. Applying the Laue theorem to the DS method, the power per unit length of diffraction circle P is given by equation (16), where m_{hkl} is the multiplicity and

$$P \propto m_{hkl} Lp \iiint I(hkl)\mathrm{d}h\mathrm{d}k\mathrm{d}l \quad (16)$$

$Lp[=(1 + \cos^2\theta)/(\sin\theta\sin 2\theta)]$ is the Lorentz-polarization factor. We obtain equations (17) and (18) and finally (19).

$$P_{CR} \propto m_{hkl} Lp \iiint \frac{\sin^2\pi N_1 h}{\sin^2\pi h} \cdot \frac{\sin^2\pi N_2 k}{\sin^2\pi k} \cdot \frac{\sin^2\pi N_3 l}{\sin^2\pi l} \bar{F}^2 \mathrm{d}h\mathrm{d}k\mathrm{d}l = m_{hkl} Lp N_1 N_2 N_3 \bar{F}^2 \quad (17)$$

$$P_{RS} \propto m_{hkl} Lp \iiint \frac{\sin^2\pi N_1 h}{\sin^2\pi h} \cdot \frac{\sin^2\pi N_2 k}{\sin^2\pi k} N_3 \sum_m \Phi_m \exp(2\pi i l m)\mathrm{d}h\mathrm{d}k\mathrm{d}l = m_{hkl} Lp N_1 N_2 N_3 \int \sum_m \Phi_m \exp(2\pi i l m)\mathrm{d}l \quad (18)$$

$$P \propto m_{hkl} Lp N_1 N_2 N_3 [\bar{F}^2 + \int \sum_m \Phi_m \exp(2\pi i l m)\mathrm{d}l] \quad (19)$$

These equations indicate that the intensities of the two types of reflections, P_{CR} and P_{RS}, can be compared on the same scale. Employing the probability functions for the random stacking,[25,33,34] the intensity arising from the random stacking is expressed by equation (20), where h and k are integers ($h - k = 3n \pm 1$), whereas l is a continuous variable. The intensity expression for the usual Laue–Bragg reflections is given by equation (21), where h, k and l are integers and $h - k = 3n$.

$$\sum_m \Phi_m \exp(2\pi i l m) = \frac{F_V^2 + F_{\bar{V}}^2}{2} - \frac{(F_V^2 + F_{\bar{V}}^2 - 4F_V F_{\bar{V}})(1 + 2\cos 2\pi l) - 2\sqrt{3}(F_V^2 - F_{\bar{V}}^2)\sin 2\pi l}{2(5 + 4\cos 2\pi l)} \quad (20)$$

$$\bar{F}^2 = \left(\frac{F_V + F_{\bar{V}}}{2}\right)^2 \quad (21)$$

Structural Model for C_xAsF_y ($8 \leqslant x < 14$, $5 \leqslant y \leqslant 6$).—As is seen from Table 4 and Fig. 7, the X-ray powder diffraction pattern for C_xAsF_y is simpler than that for $C_{14}AsF_6$ and all reflections are accounted for by the unit cell with $a_0 = a_0$(graphite) and $c_0 = I_c$. Since the staggering of carbon layers requires c_0 to be a multiple of I_c and an ordered arrangement of the AsF_y species in the gallery requires a_0 to be larger than a_0(graphite), the carbon layers are eclipsed, and the guest species are randomly placed.* In terms of the c axis, because of the geometrical restrictions imposed by the guest species, the As atoms are at the midpoint of the enclosing carbon layers, and the fluorine atoms *ca.* 1.0 Å above and below the midpoint.† The anisotropic thermal parameters used for the calculation are summarized in Table 5. In this case U_{11}(As) and U_{11}(F) were made > 2 to simulate their smeared-out distribution parallel to the *ab* plane. Alternatively, the As and F contributions can be neglected except for (00*l*). The simulated pattern based on this model for C_xAsF_y is shown in Fig. 7. The observed low-angle halo in this case is solely attributable to the quartz capillary shown by a dotted line. The agreement with the observed pattern is excellent. This model is in accordance with the room-temperature ^{19}F NMR data,[4,5,36,37] which indicate a motionally narrowed line. It is also in harmony with the electron density distribution along the c axis reported by Markiewicz *et al.*[38] for a large I_c stage-two $C_{16}AsF_5$ material. Indeed, qualitatively, the same pattern occurs for a wide range of stoichiometries, covered by the formula C_xAsF_y ($8 \leqslant x < 14$, $5 \leqslant y \leqslant 6$).

Carbon Layer Stacking Sequences.—In the single-crystal structure study of a stage-two $C_{16}AsF_5$ material, Markiewicz *et al.*[38] concluded that the carbon-layer stacking sequence AB with frequent twinning to give a situation such as ABAB . . . AB/BABA . . . BA/AB . . . was adopted. Their lattice constants were given as $a_0 = 2.46$ and $c_0 = 11.50$ Å. The present study suggests that, because the sample was not evacuated, it was rich in AsF_5 and AsF_3 neutrals. The I_c distance was large (the c_0 value of 11.50 Å corresponds to an I_c distance of 8.15 Å of the stage-one phase), therefore, the guest species were unlikely to be nestled, and the carbon layers enclosing the guest species tend to be eclipsed. Such a tendency is likely to be the cause of the frequent twinning. Although they did not specify the intercalate layers, the above sequence could be written as AB|AB . . . AB|BA|BA . . . BA|AB denoting the intercalate layers by |. The observed occurrence of streaking along [001] for the series of reflections with $h - k \neq 0$ may have been caused not only by the twinning, but also by the participation of the third type of the carbon layer, C (among A, B and C), leading to a random stacking of the carbon layers. Homma and Clarke[31] also draw the same conclusion on $SbCl_5$–graphite intercalation compounds, *i.e.*, the graphite stacking sequence for all stages is ABAB with stacking faults in the same sense as the 'twinning' used by Markiewicz *et al.*[38] Although they were able to fit the data for stages 3–5, no good agreement was obtained for stage one. The related work done on stage-one $C_{16}AsF_6$[17] has shown

* With the I_c distance of 8.0 Å, the guest species have more vibrational freedom than in the nestled AsF_6 structure. Trigonal-bipyramidal AsF_5 can undergo Berry pseudorotation (see ref. 35) and AsF_3 may undergo inversion or freely rotate. Because of these movements, each species approaches large sphere character. Maximum accommodation for the 'jelly fish' guests is provided in the cavity between eclipsed hexagons. This may be the reason for the carbon-layer eclipsing. The guest species, probably, have also some translational freedom, which explains $a_0 = a_0$(graphite).

† In the case of AsF_3, the lone electron pair also constrains the As atoms to be near the mid-plane of the carbon layers.

a clear three-dimensional structure at lower temperatures with an A|B|A|B . . . carbon stacking sequence. It is possible that the room-temperature stage-one C–$SbCl_5$ has an intermediate structure of $C_{14}AsF_6$, $C_{16}AsF_6$ and C_xAsF_y, provided that $SbCl_6^-$ plays an active role and can nestle. Vaknin and Fischer[39] concluded that their stage-two $C_{16}AsF_5$ has an AB|CA|BC stacking sequence without the twinning mentioned by Markiewicz *et al.*

In the above three cases it is not certain whether the AB stacking sequence is a consequence of the nestling of MX_6^- species. However, many other (pseudo) O_h or T_d fluoro-, oxo- or oxofluoro-ligand guest species will be found to nestle in the graphite layers, if the guest concentration is sufficiently low to permit it. Diffraction data on $C_8^+SO_3F^-$ obtained in these laboratories[40] indicate that the SO_3F^- are nestled. A small I_c distance is a strong indicator of such nestling but the impact upon the X-ray diffraction, of both the staggering of the enclosing carbon sheets, and their random stacking, should also signal occurrence of nestling. Clearly neutral guest species, because they are not strongly attracted to the carbon sheets, will be less likely to nestle than anions. Also when the guest concentration exceeds a critical value, nestling will no longer be possible. In that situation the most commodious arrangement of the enclosing carbon sheets appears to be the eclipsed one.

Experimental

Apparatus.—Most preparations were carried out in a stainless steel cell attached *via* Swagelock fittings to a stainless steel Whitey IKS4 valve. Some reactions were carried out in FEP (Chemplast, Inc.) tubes. All of the solid materials were handled in the dry atmosphere of a Vacuum Atmospheres Corporation Drilab. Volatiles are manipulated with a Monel-metal and stainless-steel vacuum line provided with Autoclave Engineering 30VM-6071 valves.

Reagents.—Two kinds of graphite were used: Union Carbide SP-1 graphite powder and Union Carbide highly oriented pyrolytic graphite (HOPG). The latter was used for X-ray pre-absorption edge studies, and the former for all other reactions. The graphite was pre-treated by heating it to *ca.* 1500 °C in a dynamic vacuum. Arsenic pentafluoride (Ozark–Mahoning) was purified by vacuum distillation from a trap at −78 °C to one at −196 °C, followed by evacuation of volatiles at −126 °C, and was checked for purity by IR spectroscopy. Dioxygen(1 +) hexafluoroarsenate was prepared by the standard procedure.[41]

Instrumentation.—The IR spectra were recorded with a Perkin Elmer model 597 spectrometer over the range 200–4000 cm^{-1}. The cell was of Monel metal and had a 10 cm path length with silver chloride windows. Debye–Scherrer X-ray powder diffraction patterns were obtained using a General Electric Co., Precision Camera (circumference 45 cm), using nickel-filtered Cu-Kα radiation. Powdered samples were loaded into 0.5 or 0.7 mm diameter thin-walled quartz capillaries (Charles Supper Company, Inc.) in the Drilab. Guinier–Simon photographs[26] were obtained at Max-Planck-Institut für Festkörperforschung, Stuttgart, Germany. X-Ray absorption experiments were carried out at the Stanford Synchrotron Facility, Palo Alto, USA.

Chemical Analyses.—Routine CHN analyses were performed on all samples by the Microanalytic Laboratory in the College of Chemistry, University of California, Berkeley, USA. Some samples (given in Table 1) were fully analysed by Galbraith Laboratories, Inc. (Knoxville, TN, USA); C, H, N, As, F and O analyses being carried out.

Procedure.—For each reaction *ca.* 100 mg of graphite were used.* The products of reaction were subjected to a dynamic vacuum for 0–500 h at room temperature. Volatiles were trapped at −196 °C and were examined by IR spectroscopy.

Interaction of Graphite with Gaseous AsF_5.—(*a*) *Single treatment with* AsF_5. Graphite was transferred to the pre-weighed cell in the Drilab. Excess of AsF_5 ($C:AsF_5 < 8:1$) was condensed on to the graphite at −196 °C, and the quantity was determined by gravimetry.† The mixture in the small volume cell was warmed to room temperature and was shaken mechanically overnight.

(*b*) *Repeated treatment with* AsF_5. In some experiments graphite was repeatedly treated with AsF_5. After the initial cycle, which was the same as the single treatment described above, the remaining gases were removed and the sample was exposed to a dynamic vacuum overnight. In the second and later cycles, a relatively large amount of AsF_5 was used (molar ratio $C:AsF_5 \approx 8:1$). Each overnight reaction was followed by an overnight evacuation in a dynamic vacuum, and the cycle was repeated 4 to 8 times. The volatiles from the sample in the first cycle were, of course, the same as the above section (*a*), and were discussed in the Results and Discussion section. In the second and later cycles, after removal of the non-intercalated gases (which contained some AsF_3 and a large amount of AsF_5), only AsF_3 was observed in the volatiles. After the third–fourth cycles, the amount of AsF_3 in the volatiles became very small.

(*c*) *Samples for synchrotron radiation studies.* Highly oriented pyrolytic graphite chips of *ca.* 0.1 mm thickness were used for X-ray arsenic pre-absorption edge studies. The sample $C_{19}AsF_6$ shown in Fig. 3 was prepared by treating graphite with AsF_5 followed by evacuation in a dynamic vacuum. The arsenic K(1s ⟶ 4p) pre-absorption edge region was studied.

Interaction of Graphite with Gaseous AsF_5 *and* F_2.—The interaction of graphite with $AsF_5 + F_2$ was carried out in a manner similar to the preparations involving graphite and AsF_5 alone. Large amounts of AsF_5 and F_2 (molar ratios $C:AsF_5 < 8:1$ and $AsF_5:F_2 < 2:1$) were condensed consecutively on to the graphite at −196 °C and the cell was warmed to room temperature.

Interaction of Graphite with Solid O_2AsF_6.—(*a*) *Direct mixing at room temperature.* Graphite powder and solid (powder) O_2AsF_6 were mixed and mechanically agitated. The reactions were run for 1–6 d. When the relative amount of O_2AsF_6 was small, the amount of evolved gas corresponded well to that of oxygen produced according to reaction (22). When an excess

$$xC + O_2AsF_6 \longrightarrow C_xAsF_6 + O_2 \qquad (22)$$

amount of O_2AsF_6 ($C:O_2AsF_6 <$ *ca.* 10:1) was used, some O_2AsF_6 was left unreacted.

(*b*) *Reaction at an elevated temperature.* Some of the graphite–O_2AsF_6 reactions were run by keeping the solid mixture at 60 °C for 1–6 d. Unreacted AsF_5 and F_2 (and O_2) from the decomposition of O_2AsF_6 were removed by evacuation.

(*c*) *By decomposition of* O_2AsF_6. Graphite and O_2AsF_6 were

* For gravimetric work a larger amount of graphite was preferred, but it was found, in the course of the study, that if the sample size much exceeded 100 mg, it was difficult to maintain the efficient mixing of the solid and gaseous reactants, necessary for high homogeneity of the product.

† Tensimetry provided a rough measure of the amount of AsF_5 to be transferred. Whenever AsF_5 was transferred in the vacuum line, an appreciable pressure drop [*e.g.* from 700 to 650 Torr (93 100–86 450 Pa)] was observed over a period of a few seconds, after which the pressure stayed constant. Such a pressure decrease was not observed with PF_3, for example. See footnote ‡ on p. 2081 for the explanation of this ready absorption of AsF_5 by the inner wall of the vacuum line.

placed separately in a T-shaped cell, and the O_2AsF_6 was decomposed at *ca.* 120 °C while leaving the graphite at room temperature. Since the amount of oxygen found in the product was small (< 0.5, see Table 1), this reaction was essentially the same as $C + AsF_5 + F_2$, except that the $AsF_5:F_2$ ratio was exactly 2:1. The same may be true for the above sections (*a*) and (*b*) in the text.

Simulation of the XRPD Pattern for $C_{14}AsF_6$.—The observed values were used for a_0 and c_0, *i.e.*, $a_0 = 2.45$ and $c_0 = 7.63$ Å. To define the z coordinates, the As atoms were placed at the midpoint of the two enclosing carbon layers and the F atoms were located 1.00 Å [17] from the mid-plane in either z direction ($z_F = 1.00/7.63$). Owing to the nestling, the fluoride ligands are centred on carbon atom hexagons. Consequently the (x,y) coordinates of all atoms are either (0,0), $(\frac{1}{3},\frac{2}{3})$ or $(\frac{2}{3},\frac{1}{3})$. The C, As and F atoms are weighted by factors, 1, $\frac{1}{7}$ and $\frac{3}{7}$ to match the composition $C_{14}AsF_6$. In order to simulate the (10*l*) scattering feature the following process was carried out instead of expressing the scattering profile $P_{2\theta}$ analytically, where $P = \int P_{2\theta} d(2\theta)$, since $P_{2\theta}$ at $(2\theta)_{100}$ is infinite.[42] The integration in equation (19) was done numerically between l and $l + 0.01$ where $l = 0.01n$. Each integrated value was added to the corresponding element of the one-dimensional array, $P(2\theta)$ (dimension 900), which represents the power per 0.1° (2θ) in the range $0 < 2\theta < 90°$. The resultant power distribution for (10*l*) can be directly compared with the intensities (powers) for (00*l*) and (11*l*) reflections, *i.e.*, with the values of $\bar{F}^2$ according to equations (19) and (21). The final simulated pattern shown in Fig. 6 was obtained by giving each $P(2\theta)$ the Gaussian function with a standard deviation of 0.3° (2θ). Gaussian function was not used for the simulated patterns in Fig. 11.

Acknowledgements

We gratefully acknowledge the support of the director, Office of Energy Research, Office of Basic Energy Sciences, Chemical Sciences Division of the US Department of Energy under Contract no. DE-AC03-76SF00098. We also thank Dr. A. W. Moore of Parma Technical Center, Union Carbide Corporation for generously supplying the HOPG graphite used in these studies, and Prof. Dr. A. Simon and W. Röthenbach of MPI-FKF for taking the Guinier-Simon photographs. F. O. thanks Professor H. Touhara for helpful discussion and support in drafting the manuscript.

References

1 Lin Chun-Hsu, H. Selig, M. Rabinovits, I. Agranat and S. Sarig, *Inorg. Nucl. Chem. Lett.*, 1975, **11**, 601.
2 E. R. Falardeau, G. M. T. Foley, C. Zeller and F. L. Vogel, *J. Chem. Soc., Chem. Commun.*, 1977, 389.
3 G. M. T. Foley, C. Zeller, E. R. Falardeau and F. L. Vogel, *Solid State Commun.*, 1977, **24**, 371.
4 L. B. Ebert and H. Selig, *Mater. Sci. Eng.*, 1977, **31**, 177.
5 R. L. Kleinberg and L. B. Ebert, *Synthetic Metals*, 1980, **2**, 245.
6 J. E. Fischer, *J. Chem. Soc., Chem. Commun.*, 1978, 544.
7 M. J. Moran, J. E. Fischer and W. R. Salaneck, *J. Chem. Phys.*, 1980, **73**, 629.
8 J. W. Milliken and J. E. Fischer, *J. Chem. Phys.*, 1983, **78**, 5800.
9 N. Bartlett, R. N. Biagioni, B. W. McQuillan, A. S. Robertson and A. C. Thompson, *J. Chem. Soc., Chem. Commun.*, 1978, 200.
10 N. Bartlett, B. McQuillan and A. S. Robertson, *Mater. Res. Bull.*, 1978, **13**, 1259.
11 E. R. Falardeau, L. R. Hanlon and T. E. Thompson, *Inorg. Chem.*, 1978, **17**, 301.
12 V. Münch and H. Selig, *Synthetic Metals*, 1979/80, **1**, 407.
13 H. Selig, M. J. Vasile, F. A. Stevie and W. A. Sunder, *J. Fluorine Chem.*, 1977, **10**, 299.
14 R. Pentenrieder and H. P. Boehm, *Rev. Chim. Minéral.*, 1982, **19**, 371.
15 P. A. W. Dean, R. J. Gillespie, R. Hulme, *Chem. Commun.*, 1969, 990.
16 J. O. Besenhard and H. P. Fritz, *Angew. Chem., Int. Ed. Engl.*, 1983, **22**, 950.
17 F. Okino, Y. Sugiura, H. Touhara and A. Simon, *J. Chem. Soc., Chem. Commun.*, 1993, 562.
18 A. Lerf and R. Schöllhorn, *Inorg. Chem.*, 1977, **16**, 2950.
19 T. Mallouk, Ph.D. Thesis, University of California, Berkeley, 1983.
20 N. Bartlett, F. Okino, T. E. Mallouk, R. Hagiwara, M. Lerner, G. L. Rosenthal and K. Kourtakis, *Adv. Chem.*, 1990, **226**, 392.
21 M. Lerner, R. Hagiwara and N. Bartlett, *J. Fluorine Chem.*, 1992, **57**, 1.
22 A. A. Woolf, *J. Fluorine Chem.*, 1980, **15**, 533.
23 T. E. Mallouk, G. L. Rosenthal, G. Müller. Brusasco and N. Bartlett, *Inorg. Chem.*, 1984, **23**, 3162.
24 G. L. Rosenthal, T. E. Mallouk and N. Bartlett, *Synthetic Metals*, 1984, **9**, 433.
25 F. Okino, Ph.D. Thesis, University of California, Berkeley, 1984.
26 A. Simon, *J. Appl. Crystallogr.*, 1971, **4**, 138.
27 N. Bartlett, E. M. McCarron, B. W. McQuillan and T. E. Thompson, *Synthetic Metals*, 1979/80, **1**, 221.
28 N. Bartlett, B. G. DeBoer, F. J. Hollander, F. O. Sladky, D. H. Templeton and A. Zalkin, *Inorg. Chem.*, 1974, **13**, 780.
29 J. A. Ibers, *Acta Crystallogr.*, 1956, **9**, 967.
30 R. W. G. Wyckoff, *Crystal Structures*, Interscience, New York, London, 1963, vol. 1, pp. 26, 27.
31 H. Homma and R. Clarke, *Phys. Rev. B*, 1985, **31**, 5865.
32 See, (*a*) L. V. Azároff, *Elements of X-Ray Crystallography*, McGraw-Hill, New York, 1968; (*b*) A. Guinier, *X-Ray Diffraction*, Freeman, San Francisco and London, 1963; (*c*) B. E. Warren, *X-Ray Diffraction*, Addison-Wesley, Reading, MA, 1969; (*d*) W. H. Zachariasen, *Theory of X-Ray Diffraction in Crystals*, Wiley, New York, 1945.
33 F. Okino, unpublished work.
34 Ref. 32(*b*), pp. 226–231.
35 F. A. Cotton and G. Wilkinson, *Advanced Inorganic Chemistry*, Wiley, New York, 4th edn., 1980, pp. 1219–1221.
36 L. B. Ebert, D. R. Mills and J. C. Scanlon, *Mater. Res. Bull.*, 1979, **14**, 1369.
37 B. R. Weinberger, J. Kaufer, A. J. Falardeau and J. E. Fischer, *Solid State Commun.*, 1978, **27**, 163.
38 R. S. Markiewicz, J. S. Kasper and L. V. Interrante, *Synthetic Metals*, 1980, **2**, 363.
39 D. Vaknin and J. E. Fischer, *Synthetic Metals*, 1988, **23**, 101.
40 R. N. Biagioni, Ph.D. Thesis, University of California, Berkeley, 1980.
41 J. Shamir and J. Binenboym, *Inorg. Chim. Acta*, 1968, **2**, 37.
42 Ref. 32(*a*), pp. 279–281.

Received 7th December 1992; *Paper* 2/06484G